Ab initio study of the electronic properties and thermodynamic stability of supported and functionalized two-dimensional Sn films

Ana Suarez Negreira,* William G. Vandenberghe, and Massimo V. Fischetti
Department of Materials Science and Engineering, University of Texas, Dallas, Richardson, Texas 75080, USA
(Received 5 November 2014; revised manuscript received 12 May 2015; published 3 June 2015)

Using density-functional theory (DFT), we study the growth of pristine and functionalized tin monolayers (Sn-MLs) on three different substrates, CdTe, InSb, and Si(111), and the impact these substrates have on the topological insulating properties of the electronic band structure. The presence of the substrate leads to strain and electronic charge transfer, which cause significant changes in the stability and electronic properties of the supported Sn-ML. Growth of pristine Sn-MLs on Si(111) leads to metallic behavior resembling that of the high-buckled Sn-ML phase; pristine Sn-MLs grown on InSb do not maintain a gap throughout the entire Brillouin zone; and pristine Sn-MLs grown on CdTe are unlikely to exhibit an experimentally observable gap. Provided the charge transfer from the substrate can be compensated, halogen-functionalized Sn-MLs grown on CdTe and InSb are topological insulators, albeit with a reduced band gap compared to their free-standing counterparts (from 0.34 eV for Sn-ML-I to 0.17 eV for InSb-Sn-ML-I). We employ *ab initio* thermodynamics calculations to study the thermodynamic stability of the halogenated InSb-Sn-MLs and CdTe-Sn-MLs surfaces for a temperature range of 100–1000 K under two extreme environments: ultrahigh vacuum (used in most of the laboratory characterization techniques) and rich-halogen conditions (10% vol. halogen environment). Our results indicate that it is possible to obtain stable topologically insulating Sn-MLs grown epitaxially on lattice-matched substrates.

DOI: 10.1103/PhysRevB.91.245103 PACS number(s): 68.90.+g, 73.43.−f

I. INTRODUCTION

The future of electronic applications such as nanotransistors may benefit from the development of two-dimensional (2D) materials [1] with a band gap larger than $k_B T$ and with robust electronic properties that must be preserved in large-scale production. A candidate for such a material includes tin monolayers (Sn-MLs), with the tin in a low-buckled hexagonal configuration, coined "stannene" and "stannanane" (since stannane is SnH_4) in recent studies [2,3]. In this paper we employ stannene, stannanane, and halostannanane to refer to pristine Sn-MLs, Sn-MLs functionalized with hydrogen, and Sn-MLs functionalized with halogens, respectively.

In the absence of spin-orbit coupling (SOC), the stannene band structure resembles the graphene band structure with a Dirac cone at the K point. But since Sn is much heavier than C, SOC effects are important and a significant band gap appears when SOC effects are included, making it a room-temperature topological insulator [4–6]. The robustness of the topological properties gives Sn-MLs an advantage for nanotransistors compared to the "fragile" graphene properties which degrade in the presence of crystal defects (e.g., grain boundaries or surface roughness significantly decrease the large conductivity of pristine graphene [7–9]). Furthermore, by gating ribbons, one can control the current over more than 3 orders of magnitude, enabling the use of these materials for transistor applications [10].

Previous theoretical studies have focused on free-standing Sn-MLs to obtain tin-based topological insulators [11,12] but, in practice, growth on a lattice-matched substrate is desired since free-standing stannene favors the adoption of a high-buckled, metallic, configuration [13].

Experimentally, the growth of ultrathin tin films has focused on the growth of α-Sn on InSb because of its good lattice match (only a slight compressive strain of 0.14%) [14,15]. The work by Ohtsubo *et al.* [15] reports a nearly massless electron dispersion for the 2D surface states and a band gap of 230 meV when the α-Sn(001) film growth on InSb(001) is functionalized with 1 ML of Bi. The same substrate is used by Barfuss *et al.* [16] to produce thicker strained α-Sn films that behave like 3D topological insulators. Another good lattice-matched substrate is CdTe, whose (001) surface was used by Farrow *et al.* [17] to heteroepitaxially grow α-Sn films, but their inability to grow ultrathin films led to an α-to-β-Sn phase transformation at 70 °C. Furthermore, another study showed the growth of four-monolayer-thick α-Sn on a Si(111) substrate, despite a significant lattice mismatch (19.5%) [18]. Nevertheless, a good understanding of the effect of these substrates on the electronic and structural properties of ultrathin Sn films is still lacking. For this reason, here we study theoretically the growth of a Sn monolayer on the (111) surface of InSb, CdTe, and Si. While it has been reported that α-tin(111) thin film can be grown on the reconstructed InSb(111) surfaces [19,20], the current study focuses on pristine InSb(111) as a simpler system to study the effect of substrates on the stability and electronic properties of Sn monolayers.

The structural and electronic properties of supported Sn-ML films may also be tuned through surface functionalization. Indeed, the largest topological band gap of Sn-MLs is observed upon halogen chemisorption on both sides of free-standing Sn-MLs [2,5]. Although promising electronic properties for this topological insulator are expected, little is known about its thermodynamic stability under real conditions. Therefore, the analysis of the structural and electronic properties of supported and surface-functionalized Sn-MLs needs to be complemented with a study of their thermodynamic stability. For this purpose we employ *ab initio* thermodynamics calculations including entropy, temperature, and pressure effects

*anasn@alumni.stanford.edu

to study the thermodynamic stability of these systems under two extreme environments: ultrahigh vacuum (used in most of the laboratory characterization techniques) and rich-halogen conditions (10% vol. halogen environment).

The paper is organized as follows: In Sec. II we describe the methodology employed. In Sec. III we deal with the properties of free-standing Sn-MLs and how the topological nature of their bandstructure can be determined. Section III is divided into three subsections: Section III A analyzes the geometry and stability of the three different substrates used in this study, CdTe, InSb, and Si, all with (111) surfaces, in order to determine the optimal substrate thickness and surface termination. In Sec. III B we investigate the three supported systems: InSb-Sn-MLs, CdTe Sn-MLs, and Si-Sn-MLs. In Sec. III C, the same procedure is repeated for the functionalized supported Sn-MLs. Finally, we present our conclusions.

II. COMPUTATIONAL METHODOLOGY

Structural optimizations are performed using plane-wave DFT calculations using the Vienna *ab initio* Simulation Package (VASP) [21]. The Perdew-Burke-Enzerhoff generalized-gradient approximation (PBE and GGA) is used for the exchange-correlation functional [22]. For the CdTe, InSb, Si, and Sn bulk calculations, a projector augmented wave (PAW) [23] pseudopotential is used with an energy cutoff of 500 eV. The number of k points for the Brillouin zone integration is chosen according to a Monkhorst-Pack [24] grid of $8 \times 8 \times 8$ with a convergence criterion of 10^{-4} eV.

The surfaces of the CdTe(111), InSb(111), and Si(111) substrates and the monolayer Sn(111) are studied using an asymmetric 1×1 unit cell (i.e., the slab does not have a mirror symmetry plane parallel to the surface due to the difference between the top and bottom layers). The slabs are separated by a 15-Å-thick vacuum padding to prevent interaction between adjacent supercells and to minimize the impact of any dipole moment present. To study the slabs, an $8 \times 8 \times 1$ k-mesh is used. The positions of all atoms in the substrate are allowed to relax with the exception of the atoms in the bottom layer, which are kept fixed in their bulk positions throughout the calculations.

The bonds in CdTe are formed with 0.5 electrons from the Cd atom and 1.5 electrons from the Te atom, while the bonds in InSb are formed with 0.75 electrons from the In atom and 1.25 electrons from the Sb atom. In order to saturate the dangling bonds of the atoms in the top and bottom layers of the CdTe and InSb substrates, fictitious hydrogen atoms (hydrogen atoms with a fractional nuclear and electronic charge) are used in the following way: H atoms with a +1.5 electron charge saturate the Cd-terminated surfaces, while H atoms with a +0.5 electron charge are used for the Te-terminated surfaces. For the InSb substrate, H atoms with +0.75 and +1.25 electron charge are used to saturate the Sb- and In-terminated surfaces, respectively [25,26]. As for the Si(111) surface, the dangling bonds are passivated with "conventional" +1 electron-charge H atoms.

Whenever information was needed about gas-phase species (F_2, Cl_2, Br_2, and I_2), these are modeled as isolated molecules in a $20 \times 20 \times 20$ (Å^3) periodic box.

To assist with the symmetry classification we employed QUANTUM ESPRESSO [27] and we use the notation from Ref. [28] for the irreducible representations of the point groups describing the symmetry of the different bands under study.

III. UNSUPPORTED STANNENE AND HALOSTANNANANE

A. Geometry and band structure

The optimization of unsupported stannene and halostannanane systems is performed first to obtain a reference state for the supported monolayers. The crystal structure of the pristine and halogenated Sn-MLs with their respective band structures are shown in Fig. 1. The optimization of the two-dimensional hexagonal lattice of Sn-ML results in a lattice constant of 4.70 Å, a Sn-Sn bond distance of 2.84 Å, and a buckling distance of 0.84 Å, values that are in agreement with previous DFT studies [4,5,29]. As shown previously, the SOC induced minimum band gap is at the K symmetry point for unfunctionalized stannanane, while it is at the Γ symmetry point and has an increased magnitude (from 0.07 to 0.3 eV) upon functionalization with halogens due to the saturation of the π orbital [2,5].

The stability of the functionalized Sn-MLs is studied through the formation energies calculated as:

$$E_{\text{form}} = \frac{E_{(\text{Sn-ML-X})} - (E_{(\text{Sn-ML})} + N_{\text{X}} E_{\text{X}})}{N_{\text{X}}}, \qquad (1)$$

where $E_{(\text{Sn-ML-X})}$, $E_{(\text{Sn-ML})}$, and E_{X} are the total energy of a double-side halogenated Sn-ML (as shown in Fig. 1), the energy of the pristine Sn-ML, and the binding energy per atom of a halogen molecule, respectively. The formation energies, changes of the lattice constant of the Sn-MLs, and the SOC-induced band gaps upon halogen chemisorption are summarized in Table I.

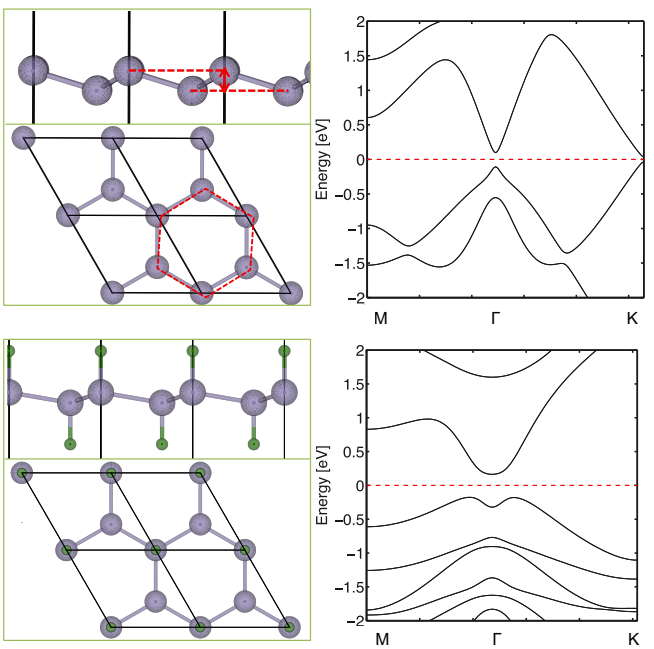

FIG. 1. (Color online) Top: Side and top views of the crystal structure (left) and band structure (right) calculated accounting for SOC for pristine unsupported stannanane. Bottom: The same but for stannanane functionalized with I. The horizontal dashed lines (red online) in the right frames indicate the Fermi level.

TABLE I. Calculated structural parameters and binding energies of pure and halogenated Sn-ML systems. The data in parentheses correspond to previous calculations [5].

System	Band gap (eV)	E_{form} (eV)	Lattice constant (Å)
Sn-ML	0.07(0.07)	NA	4.70(4.67)
Sn-ML-F	0.29(0.37)	−3.38(−3.34)	5.03(4.94)
Sn-ML-Cl	0.29(0.35)	−1.80(−1.68)	4.94(4.93)
Sn-ML-Br	0.29(0.39)	−1.58(−1.46)	4.89(4.91)
Sn-ML-I	0.34(0.48)	−1.25(−1.13)	4.89(4.89)

As shown in Table I, the binding strength of halogens on unsupported Sn-MLs and the geometrical strain generated on the film structure (as indicated by the variation of its lattice constant) decrease from F to I. For the electronic structure, I chemisorption leads to the largest band gap, in agreement with previous theoretical results [2,5].

B. Band symmetry analysis

To improve our understanding of the electronic structure of Sn-MLs and their topological nature, we analyze the symmetry and orbital properties of the stannene, stannanane, and halostannanane bands and contrast them with those of graphene.

Carbon and tin atoms each have four valence electrons, whereas the halogens such as iodine have seven valence electrons. The point group describing the graphene symmetry is D_{6h}, while graphanelike compounds like stannanane and halostannanane have a reduced D_{3d} symmetry because of the absence of a vertical mirror plane. On a support, stannanane further loses its inversion symmetry and the symmetry reduces to C_{3v}.

To determine whether the compounds are topological insulators, we employ Fu's criterion (for TI $\nu = 1$)

$$(-1)^{\nu} = \prod_i \delta_i, \tag{2}$$

where δ_i are the parity eigenvalues for a material with inversion symmetry and i runs over Γ and 3 M points [30].

For supported stannanane, Eq. (2) can be used as well but now with δ_i the parity eigenvalues for mirror symmetry. To prove the latter statement, it is satisfactory to see that the Berry curvature $\mathcal{F}(\mathbf{k}) = \nabla_{\mathbf{k}} \times \mathcal{A}(\mathbf{k})$ vanishes at the edge of the hexagonal Brillouin zone and along the K-Γ axis because of mirror symmetry. This enables the choice of a gauge for Berry's potential $\mathcal{A}(\mathbf{k}) = 0$, as outlined in Ref. [30], along a path connecting the M points and Γ.

In Table II, we show the symmetry analysis of the different valence bands and the first conduction band in the absence of spin-orbit coupling. Inspecting the character table and knowing the representations subscripted by g and u are even and odd under inversion, respectively, the criterion given in Eq. (2) yields $\delta_\Gamma = -1$ and $\delta_M = 1$ for graphene, stannanane, and halostannanane, making them topological insulators ($\nu = 1$).

For graphene and stannene, each cell has eight valence electrons and at K the E band is degenerate and half occupied in the absence of spin-orbit coupling. For graphene, this results in the well-known Dirac cone, while for stannene the spin-orbit coupling results in a significant topological band gap. For halostannanane, each cell has 22 electrons occupying 11 twofold degenerate bands; in the absence of spin-orbit coupling the E_g band is half occupied at Γ and spin-orbit opens a band gap exceeding 300 meV at room temperature. In stannanane, the A_{2u} band energy lies above that of the E_g band at Γ, making $\delta_\Gamma = \delta_M = -1$ and stannanane a trivial insulator ($\nu = 0$). The emerging interpretation is that if functionalization can lower the energy of the A_1 band compared to the E band in supported structures, the functionalized structure will be a topological insulator; otherwise, it will be a trivial insulator as indicated in Table II.

TABLE II. Symmetry classification of all occupied bands and one unoccupied band at the Γ, K, and M points in graphene, stannene, stannanane, and halostannane. Functionalized stannanane is a topological insulator when the energy of the E band lies above that of the A_1 band at Γ.

Graphene (8 electrons/unit cell)					
Γ (D_{6h})	A_{1g}	A_{2u}	E_{2g}	E_{2g}	A_{1g}
M (D_{2h})	B_{2u}	A_g	B_{3u}	B_{3g}	B_{1u}
K (D_{3h})	E'	E'	A_1'	E''	E''
Stannene (8 electrons/unit cell)					
Γ (D_{3d})	A_{1g}	A_{2u}	E_g	E_g	A_{2u}
M (C_{2h})	B_u	A_g	A_u	A_g	B_u
K (D_{3h})	E	E	A_1	E	E
Stannanane (10 electrons/unit cell)					
Γ (D_{3d})	A_{1g}	A_{2u}	A_{1g}	E_g	E_g	A_{2u}
M (C_{2h})	B_u	A_g	A_g	B_u	A_u	A_g
K (D_{3h})	E	E	E	E	A_1	E
Halostannanane (22 electrons/unit cell)											
Γ (D_{3d})	A_{1g}	A_{2u}	A_{1g}	A_{2u}	A_{1g}	E_g	E_g	E_u	E_u	A_{2u}	E_g	E_g
M (C_{2h})	B_u	A_g	B_u	A_g	A_g	B_u	A_u	B_u	A_g	B_g	A_u	A_g
K (D_{3h})	E	E	E	E	A_1	E	E	A_2	E	E	A_1	E
Trivial stannanane					
Γ (C_{3v})	·	E	E	A_1	
M (C_s)	·	A'	A'	A''	
K (C_3)	·	E^*	E	A	
Topological stannanane					
Γ (C_{3v})	·	A_1/E	E/A_1	E	
M (C_s)	·	A'	A'	A''	
K (C_3)	·	E^*	E	A	

An alternative interpretation of the halostannanane band structure is possible when we model the effect of the halogens as each removing one electron from the stannene. If stannene only has six electrons in each unit cell rather than eight, its E_g band is only half occupied at Γ while the E band at K is empty.

A last question we investigate in this section is whether the classification of the topological nature is maintained when improved band-structure calculation methods are used. In fact it is well known that band-structure results obtained using GGA DFT do not accurately predict the band gap. Therefore,

we perform a G_0W_0 analysis for unsupported stannanane and halostannanane and observe that the band order is maintained, whereas the gap at Γ increases from 0.48 to 0.9 eV for iodostannanane and from 0.27 to 0.5 eV for stannanane. For the supported structures studied in the following section, the G_0W_0 calculations are computationally prohibitive but the results obtained for the free-standing Sn-MLs indicate that the use of GGA DFT is a good indicator of the topological nature of a structure.

IV. SUPPORTED STANNENE AND STANNANANE

A. Optimization and stability of substrates: CdTe(111), InSb(111), and Si(111)

The three materials chosen as possible substrates for the Sn-ML films are Si(111), CdTe(111), and InSb(111). We choose the (111) surface because it is commensurate with the hexagonal lattice of the Sn-ML, as illustrated in Fig. 2. The lattice constants resulting from the optimization of the bulk substrate (6.63 Å for CdTe, 6.65 Å for InSb, and 5.47 Å for Si) are all in agreement with previous DFT studies (6.63 Å [31], 6.64 Å [32], and 5.47 Å [33] for CdTe, InSb, and Si, respectively).

The determination of the minimum number of atomic layers needed to obtain an accurate representation of a condensed phase must be established by judging the change of interlayer distances of the (111) slab with respect to the bulk value. The interlayer spacings of the three-, four-, five-, and six-layer-slabs and their difference with respect bulk distances (in %)

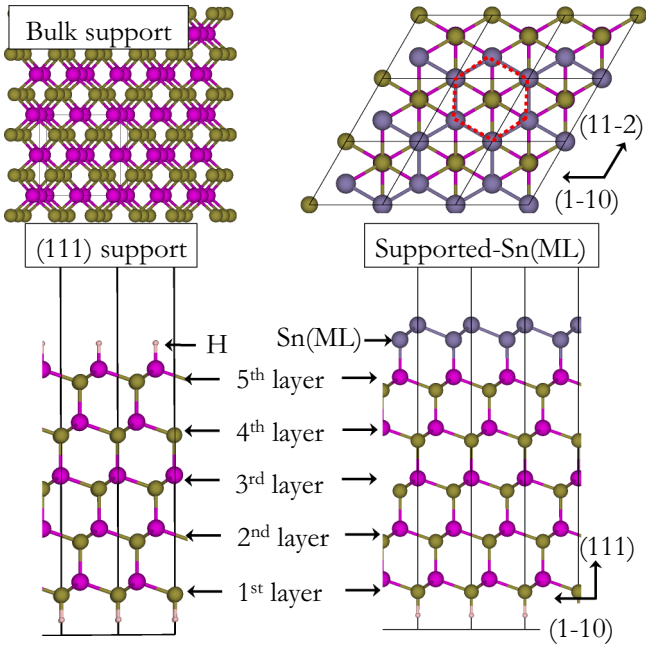

FIG. 2. (Color online) Left: Atomic structure of bulk and the (111) surface of a five-layer slab of the substrate materials: CdTe, InSb, and Si. The pink and green balls represent the substrate atoms: Cd and Te for CdTe and In and Sb for InSb. For the case of Si, there is only one color. Hydrogen atoms (small white balls) saturate the dangling bonds of top and bottom layer of the substrates. Right: Top and side views of the supported Sn-ML systems. The dashed hexagonal lattices correspond to the Sn monolayer (gray balls).

are summarized in Table III. We conclude that the use of slabs of five layers (schematically represented in Fig. 2) yields sufficient accuracy, since they exhibit an interlayer difference smaller than 5%.

A slab model representing a polar substrate such as CdTe and InSb(111) have two inequivalent terminations (top and bottom of the slab): Cd- and Te-terminated surfaces for CdTe(111) and In- and Sb-terminated surfaces for InSb(111). Therefore, the surface free-energy value obtained from a slab calculation gives an average surface energy of the two terminations. A rigorous method to determine the *absolute* free energy for polar surfaces is explained in detail in Refs. [34,35], where an infinitely long wedge with a trianglular cross section is used. *Absolute* values of surface free energy are key to determine the equilibrium morphology during a growth process of bulk and epitaxial films [35].

However, despite the mentioned limitation, the use of a slab model still can be used to determine the *relative* surface energy between the two possible surface terminations of a polar surface. These *relative* surface free energies can be obtained by using slabs with the same number and type of atoms, with a fixed bottom surface, for the different surface terminations. The dangling bonds of the top and bottom surfaces are passivated with fractionally charged hydrogen (pseudohydrogens) to avoid spurious charge transfers throughout the slab. The surface free energy of each top surface termination dictates their relative stability and is used as a selection factor in this paper.

The surface free energy is proportional to the Gibbs free energy, and the latter can be approximated to the total DFT energy as described in Ref. [36]. The surface free energy, γ, of CdTe and InSb semi-infinite slabs with two inequivalent surface is given by:

$$\gamma = \frac{1}{2A}\Big[E_{\rm syst} - N_{\rm Cd}E^{\rm bulk}_{\rm CdTe} - (N_{\rm Te} - N_{\rm Cd})\mu_{\rm Te} - N_{\rm H^{top}}\mu_{\rm H^{top}} - N_{\rm H^{bot}}\mu_{\rm H^{bot}}\Big] \quad (3)$$

and

$$\gamma = \frac{1}{2A}\Big[E_{\rm syst} - N_{\rm In}E^{\rm bulk}_{\rm InSb} - (N_{\rm Sb} - N_{\rm In})\,\mu_{\rm Sb} - N_{\rm H^{top}}\mu_{\rm H^{top}} - N_{\rm H^{bot}}\mu_{\rm H^{bot}}\Big], \quad (4)$$

where $E_{\rm syst}$ is the total energy of the five-layer slab; $E^{\rm bulk}_{\rm CdTe}$ and $E^{\rm bulk}_{\rm InSb}$ are the energy of bulk CdTe and bulk InSb per formula unit; and $\mu_{\rm Te}$, $\mu_{\rm Sb}$, and $\mu_{\rm H}$ are the chemical potentials of Te, Sb, and H, respectively. The top and bottom surfaces of the slab are passivated with different types of pseudohydrogens, which have different chemical potentials.

Since stoichiometric slabs are used as a substrate ($N_{\rm Te} = N_{\rm Cd}$ and $N_{\rm In} = N_{\rm Sb}$), these terms cancel out in Eqs. (3) and (4). For the case of zero temperature, the $\mu_{\rm H^*}$ of the different pseudohydrogen atoms simplifies to one half of the formation energy of a pseudohydrogen molecule as:

$$\mu_{\rm H^*} = \frac{E_{\rm H^*_2} - E_{\rm H^*}}{2}. \quad (5)$$

The *relative* surface free energies obtained are -0.07 eV/Å^2 for an In-terminated InSb substrate [InSb(In)], 0.05 eV/Å^2 for an Sb-terminated InSb substrate [InSb(Sb)], -0.17 eV/Å^2 for an Cd-terminated CdTe substrate

TABLE III. Change of the interlayer distance (in %) of substrate slabs with increasing number of layers with respect the bulk distances for InSb(111), CdTe(111), and Si(111) slabs.

	InSb(111)				CdTe(111)				Si(111)			
	6 lyrs.	5 lyrs.	4 lyrs.	3 lyrs.	6 lyrs.	5 lyrs.	4 lyrs.	3 lyrs.	6 lyrs.	5 lyrs.	4 lyrs.	3 lyrs.
1^{st}–2^{nd} lyr.	−0.30	−0.27	−0.30	−0.33	0.01	0.03	0.02	0.03	0.75	0.40	2.85	0.21
2^{nd}–3^{rd} lyr.	0.05	−0.05	−0.16	−0.45	0.10	−0.16	−0.17	−0.02	0.31	0.39	5.19	−3.84
3^{rd}–4^{th} lyr.	0.03	−0.06	−0.48	–	0.14	0.09	0.23	–	0.29	0.53	−2.26	–
4^{th}–5^{th} lyr.	−0.19	−0.40	–	–	0. 26	0.27	–	–	0.61	−3.45	–	–
5^{th}–6^{th} lyr.	−0.53	–	–	–	0.46	–	–	–	−3.59	–	–	–

[CdTe(Cd)], and 0.01 eV/Å^2 for an Te-terminated CdTe substrate [CdTe(Te)]. Due to their *relative* lower surface energy and resulting higher stability, we choose the InSb(In) and CdTe(Cd) terminations as substrates, along with Si(111) for the full analysis presented in this paper. For breviety, only some calculations are performed for the other two surface terminations (Te- and Sb-terminated surfaces).

B. Characterization of supported stannene

1. Geometry and thermodynamic stability

For thick layers, the different interactions between adspecies and substrate atoms, and the buildup of strain in the overlayer as the film thickness increases, produce dislocations in the supported film. However, since our aim is to study monolayer Sn films, an epitaxial growth is assumed in which the structures of the CdTe(111), the InSb(111), and the Si(111) substrates are extended to a Sn(111) termination (i.e., the atoms in the Sn-ML follow the structure of the underneath substrate). When the lattice-constant mismatch between the film and the substrate is small, even multiple layers can be grown homoepitaxially and dislocation free [37]. The relative stability of each supported Sn-ML structure is analyzed based on the formation energies, using the (1×1) five-layer H-passivated bottom-layer substrate and an unsupported Sn-ML as references. In the supported Sn-ML structure, only the bottom layer is passivated with fictitious H atoms, since the dangling bonds of the atoms of the top layer of the substrate are saturated with the Sn atoms. The binding energy of these supported Sn structures, E_{binding}, is defined as:

$$E_{\text{binding}} = E_{\text{sys}} - [E_{\text{subs}} + E_{\text{Sn-ML}}], \tag{6}$$

where E_{sys}, E_{subs}, and $E_{\text{Sn-ML}}$ are the total energies of the supported system, the H-passivated bottom layer substrate, and the unsupported monolayer Sn, respectively. The binding energies and the structural parameters of the unsupported and supported Sn-ML systems are summarized in Table IV.

TABLE IV. Calculated lattice constant a_0, lattice strain ϵ, buckling distance and formation energy of supported Sn-ML systems.

System	a_0 (Å)	ϵ (%)	Bucking (Å)	E_{binding} (eV)
Unsupported Sn	4.70	–	0.84	–
Si-Sn	3.86	−17.92	1.96	−0.10
CdTe(Cd)-Sn	4.69	−0.36	0.87	−0.83
InSb(In)-Sn	4.70	−0.06	0.89	−0.91

This table shows the predicted lattice strain on the Sn-ML film during epitaxial growth on each substrate. The binding energy is used to predict the relative stability of the different supported systems, suggesting InSb(In)-Sn ($E_{\text{binding}} = -0.91$ eV) as the most promising candidate. The much larger lattice mismatch between the Si(111) substrate and the Sn-ML is responsible for the lower stability of the epitaxial growth of α-Sn on Si(111). The predicted lattice mismatch ($\approx$18%) is in good agreement with the lattice mismatch measured experimentally (19.5%) [18]. The in-plane compression induced by the Si(111) substrate on the Sn-ML leads to a large buckling distance displacement (out of plane) of the Sn atoms compared to the unsupported Sn-ML (increasing from 0.84 Å to 1.95 Å). Despite the large lattice mismatch between Si(111) and Sn and the low stability of the supported system, there is some experimental evidence suggesting the existence of stable supported systems with up to four monolayers in thickness [18]. For this reason, in the following we further analyze the Si-Sn-ML system, along with the CdTe(Cd)-Sn-ML and InSb(In) Sn-ML systems.

2. Electronic structure

The band structures of CdTe(Cd)-Sn, InSb(In)-Sn, and Si-Sn with and without accounting for spin-orbit-coupling are shown in Fig. 3.

The Si-Sn band structure is greatly distorted compared with the band structures of the two other systems. This can be attributed to the large lattice mismatch and the geometrical constraint imposed by the Si(111) substrate and the band structure resembles that of stannene in its high-buckled phase [13]. When thicker substrates (with up to 12 atomic layers) are used for the Si-Sn system, negligible changes are observed in the band structure, indicating that the distortion of the band structure is not due to an excessively thin Si(111) substrate.

A first observation in Fig. 3 for the InSb and CdTe-supported monolayers is that the Fermi level does not fall between the conduction and valence band. This is due to the fractional charge transfer of the substrate. In this sense, monolayer-Sn supported on a polar substrate can never be a topological insulator since it is not an insulator. However, in applications where gating is possible, charge can be depleted/accumulated and the Fermi level can be moved towards the center of the gap.

But further inspection of Fig. 3 reveals that even when moving the Fermi level, stannene on InSb does not have a gap throughout the entire Brillouin zone and is therefore

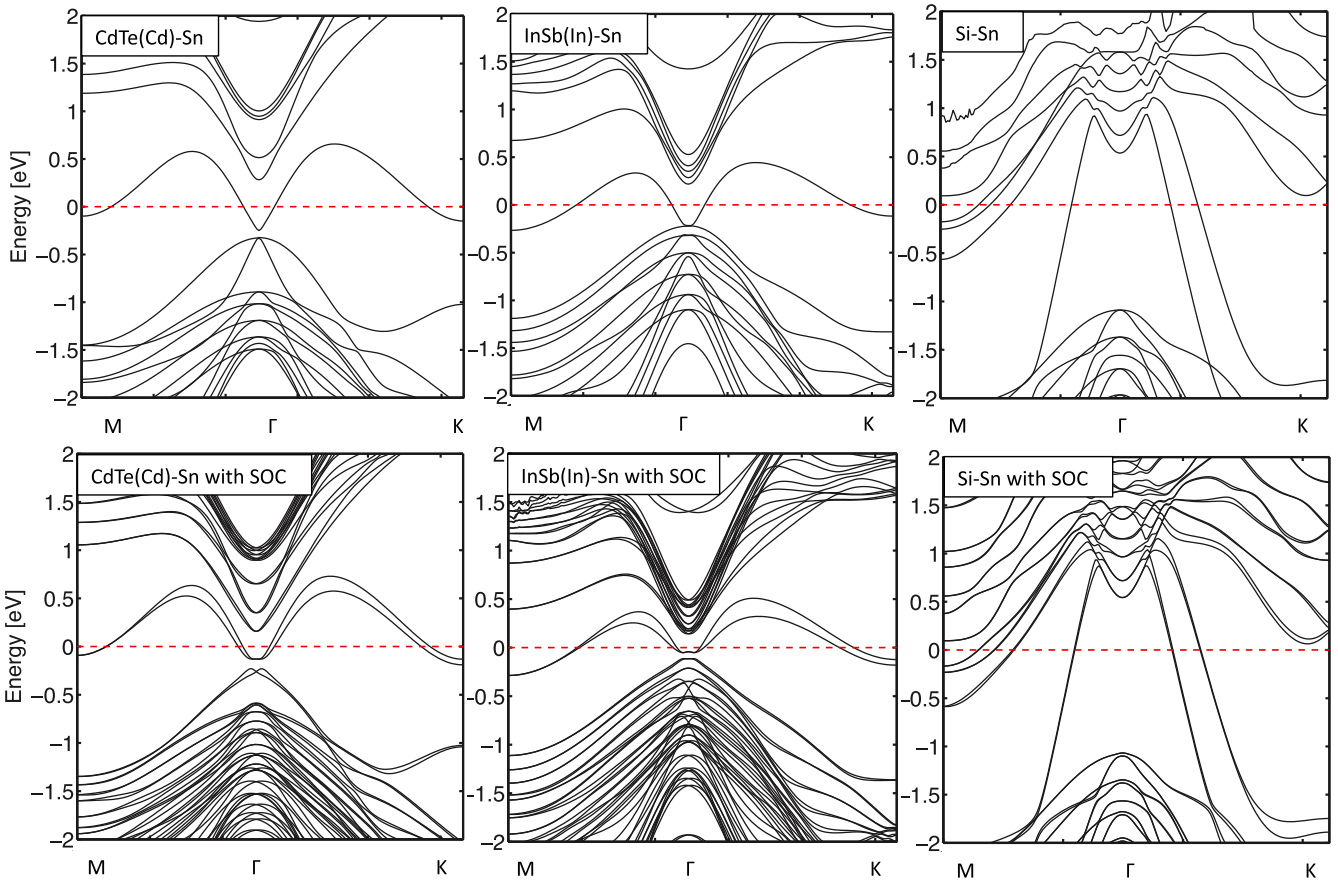

FIG. 3. (Color online) Top: Band structures for CdTe(Cd)-Sn, InSb(In)-Sn, and Si-Sn without spin-orbit-coupling effect. Bottom: Band structures with spin-orbit-coupling effect. The dashed line (red) indicates the energy of the Fermi level.

metallic, while stannene on CdTe only maintains a 0.04-eV band gap. Although the band structures for the InSb(Sb)-Sn and CdTe(Te)-Sn systems are not presented here, they showed that both systems are metallic since they lack a gap throughout the entire Brillouin zone.

An additional observation is that when the symmetry of the structure is slightly broken, the fractional occupation of the band results in convergence towards a ferromagnetic state for the calculations accounting for spin-orbit coupling. In this ferromagnetic state, stannene on both InSb and CdTe does not support a band gap throughout the entire Brillouin zone hampering the possible experimental observation of a topological gap in supported stannene. On the other hand, experimental observation of the ferromagnetic state is also unlikely, given that the energies of the ferromagnetic state do not differ significantly from those of the nonferromagnetic state.

C. Characterization of supported halostannanane

Since the largest reported gap is observed for halogen-functionalized Sn-MLs, a similar effect is expected in the supported system. A thorough analysis is performed in this section in order to quantify the effect of surface functionalization on the geometry, stability, and band structure of the InSb-Sn-ML systems (and, to a lesser extent, to halogenated CdTe-Sn-ML systems).

1. Geometry and thermodynamic stability

The first step in the analysis of the thermodynamic stability of the halogenated InSb-Sn-ML systems is the estimation of the corresponding halogen binding energies. As above, the binding energies are calculated as $E_{\text{binding}} = E_{(\text{InSbSn}-\text{X})} - [E_{(\text{InSbSn})} + E_{\text{X}}]$, an expression whose terms represent the total energy of the halogenated InSb-Sn system, of the pristine InSb-Sn system, and the binding energy per atom of a halogen molecule, respectively. The resulting binding energies are shown in Table V, which also reports the Sn-X, Sn-Sn, and Sn-In distances on the InSb(In)-Sn-ML-X system in order to quantify the geometrical changes upon functionalization.

The large binding energies of halogens on InSb-Sn-ML highlights the stability of these systems, which are slightly

TABLE V. Calculated structural parameters and binding energy of clean and halogenated InSb(In)-Sn-ML systems. Values in parentheses correspond to the CdTe-Sn-ML systems.

System	E_{binding} (eV)	Sn-X (Å)	Sn-Sn (Å)	Sn-In (Å)
InSb-Sn-ML	NA	NA	2.85	2.92
InSb-Sn-ML-F	–3.57 (–3.37)	1.95	2.87	2.87
InSb-Sn-ML-Cl	–2.00 (–1.80)	2.37	2.88	2.85
InSb-Sn-ML-Br	–1.79 (–1.60)	2.51	2.89	2.85
InSb-Sn-ML-I	–1.47 (–1.29)	2.73	2.89	2.87

higher than those determined for the CdTe-Sn-ML systems. The interaction of F with the topmost Sn atoms of the InSb-Sn-ML system leads to the strongest binding energy (−3.57 eV), while I has the lowest (−1.47 eV), following the same trend observed in the halogenated unsupported Sn-MLs. However, contrary to what was found for unsupported Sn-MLs, the adsorption of F on the InSb-Sn-ML leads to the smallest perturbation of the Sn-ML film geometry, which is measured through the changes in the Sn-Sn and Sn-In distances. A slight increase of the Sn-Sn bond distance and a contraction of the Sn-ML substrate interlayer distance (Sn-In distance) are observed upon halogen chemisorption.

The adsorption energies presented in Table V are calculated using DFT and do not give any indication of the effect of temperature or pressure on the stability of these systems. The implementation of *ab initio* thermodynamics is needed in order to include the entropic effects, important at high temperature, on the adsorption energies of halogens on the InSb-Sn-ML and CdTe-Sn-ML systems. The *ab initio* thermodynamic methodology has been explained in detail in previous studies, so here only the basic equations are presented for the case of InSb-Sn-ML system (similar equations are derived for the halogenated CdTe-Sn-ML surfaces) [36,38–40].

The stability of phases resulting from adsorption of different species on a given surface can be judged in terms of the energetic cost required to create a modified surface starting from the pristine surface [38]. The stability of different surface terminations can be evaluated from the Gibbs free energy of adsorption which, for a semi-infinite surface slab in equilibrium with a gas-phase reservoir for a given temperature and pressure, is defined as:

$$\Delta G^{\text{ads}}(T,p) = \frac{1}{A}\left[G_{\text{InSb-Sn-X}} - G_{\text{InSb-Sn}} - \sum N_{\text{X}}\mu_{\text{X}}\right], \tag{7}$$

where $G_{\text{InSb-Sn-X}}$ is the Gibbs free energy of the halogenated system, $G_{\text{InSb-Sn}}$ is the Gibbs free energy of the pristine InSb-Sn-ML surface, N_{X} is the number of gas phase halogen species, and μ_{X} is the chemical potential of the gas phase halogen (μ_{F}, μ_{Cl}, μ_{Br}, and μ_{I}). The Gibbs free energy terms in Eq. (7) are defined as $G = E_{\text{total}} + F^{\text{vib}} + F^{\text{conf}} + pV$, where the first three terms, which represents the Helmholtz free energy, are the energy at constant volume calculated with DFT, the vibrational free energy, and the configurational free energy, respectively. The last term (pV) is the free-energy contribution from the pressure-volume expansion. Previous DFT studies [38,41–43] consider that for $p < 100$ atm and $T < 1000$ K, the contributions from pressure-volume expansion (pV) and configurational free energy (F^{conf}) may be considered negligible (less than 10^{-3} meV/Å^2). Rogal and Reuter [38] also suggested that vibrational free energies of the bulk solid for both the functionalized and the pristine surfaces cancel, so only the vibrational contribution from the adsorbed species requires consideration. In this study, the vibrations associated with the Sn monolayer and adsorbed halogens are included in the surface free-energy calculations. The vibrational contributions are calculated using the harmonic oscillator approximation [38] as:

$$F^{\text{vib}}_{H_{\text{ad}}} = \sum_{k}^{3N}\left[\frac{h\omega_k}{2} + k_{\text{B}}T\ln\left(1 - e^{\frac{h\omega_k}{k_{\text{B}}T}}\right)\right] \tag{8}$$

in which the sum is over the vibrational modes, ω_k, of each of the N-adsorbed halogen atoms and Sn atoms. The vibrational modes are obtained from running the vibrational frequently calculation, where only the halogen and Sn atoms are allowed to vibrate in the direction perpendicular to the surface. The temperature and pressure dependence of the chemical potential of the gas-phase halogen species [38] are described as:

$$\mu_i(T,p) = E_i^{\text{tot}}(\text{DFT}) + E_i^{\text{ZPE}} + \mu_i(T,p_0) + k_{\text{B}}T\ln\left(\frac{p}{p_0}\right), \tag{9}$$

where $\mu_i(T,p_0)$ can be obtained from the NIST-JANAF thermochemical tables at standard pressure p_0, 1 atm [44]; E_i^{ZPE} arises from the zero-point vibrations and E_i^{tot} is the total energy obtained through the DFT calculations of a halogen molecule in a $20 \times 20 \times 20$ (Å^3) periodic box.

The thermodynamic stability of the halogenated InSb-Sn-ML and CdTe-Sn-ML surfaces are studied under two extreme environments: Ultrahigh vacuum (for partial pressures of any gas-phase species, $p_{\text{X}} = 10^{-10}$ atm) and rich-halogen conditions ($p_{\text{X}} = 10\%$ vol. for the halogen species). The first case is important because a great number of the spectroscopy techniques [e.g., x-ray photoelectron spectroscopy (XPS), Auger electron spectroscopy (AES), or time-of-flight secondary ion mass spectroscopy (ToF-SIMS)] used for surface characterization of these materials in the laboratory require ultra-high vacuum conditions. Under these conditions, weak adsorbed species (physisorbed) are no longer stable on the surface so they are not detected during the surface analysis. Therefore, it is essential to predict the stability of these halogenated systems when exposed to these common environmental conditions. On the other hand, a higher stability of these halogenated systems could be obtained by exposing these materials to a halogen-rich atmosphere, therefore preserving the surface properties caused by halogen chemisorption. The thermodynamic stability of halogenated InSb-Sn-ML and CdTe-Sn-ML surfaces as a function of temperature (100 K to 1000 K) under these two extreme environments are presented in Fig. 4, where the lowest energy corresponds to the most thermodynamically stable system.

Note how F adsorption on both types of surfaces leads to the most stable functionalized surfaces at any temperature under UHV and halogen-rich conditions, thanks to the strong adsorption energy of F, as shown in Table V. As the adsorption energies decrease from F to I, the same effect is observed on the thermodynamic stability as a function of temperature and pressure. The weakest adsorption energy corresponds to the case of I, which becomes unstable under UHV conditions for temperatures above 600 K and 500 K for InSb-Sn-ML and CdTe-Sn-ML, respectively, while under halogen-rich conditions, the same I-terminated surfaces are stable at temperatures below 900 K and 800 K. Overall, at room temperature (marked by a vertical line), all halogenated

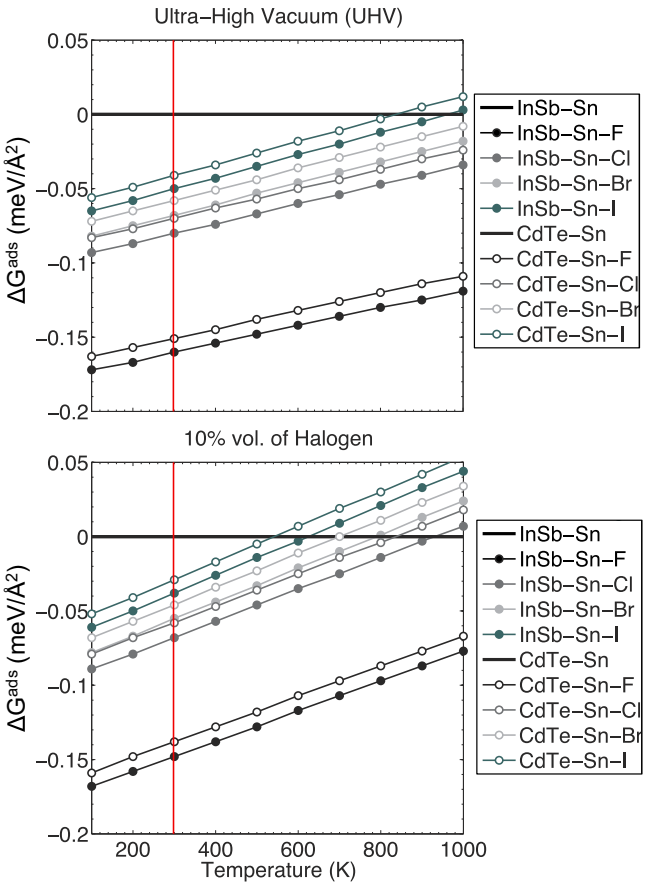

FIG. 4. (Color online) Temperature dependence of the adsorption energies of halogens on the surfaces of the InSb-Sn-ML (filled symbols) and CdTe-Sn-ML (empty symbols) systems under ultra-high vacuum (left) and halogen-rich (right) conditions. The vertical line (red) shows room temperature (298 K), while black horizontal line represents pristine InSb-Sn-ML and CdTe-Sn-ML surfaces. The more negative adsorption energies correspond to more thermodynamically stable systems.

InSb-Sn-ML and CdTe-Sn-ML systems are predicted to be stable for both types of environmental conditions.

2. *Electronic structure*

The band structure of InSb-Sn-ML-I is compared with the band structure of CdTe-Sn-ML-I, with and without inclusion of spin-orbit coupling in Fig. 5.

From Fig. 5 it is immediately clear that InSb-Sn-ML-I is a topological insulator and that the twofold degenerate E band lies above the A_1 band as discussed in Sec. III B. For CdTe-Sn-ML-I the E band is degenerate and lies below the A_1 band in the absence of spin-orbit coupling. However, when analyzing the symmetry of the wave functions after spin-orbit coupling, it is clear that the first conduction band is an E band and the last valence band is an A_1 band, making CdTe-Sn-ML-I a topological insulator as well as InSb-Sn-ML-I.

The band gap of InSb-Sn-ML-X is 0.15, 0.14, 0.15, and 0.17 eV for F, Cl, Br, and I adsorption on InSb-Sn-ML, respectively. The same values were obtained for the band gaps of halogenated CdTe-Sn-ML (0.15, 0.14 0.15, and 0.17 eV for F, Cl, Br, and I adsorption on CdTe-Sn-ML, respectively).

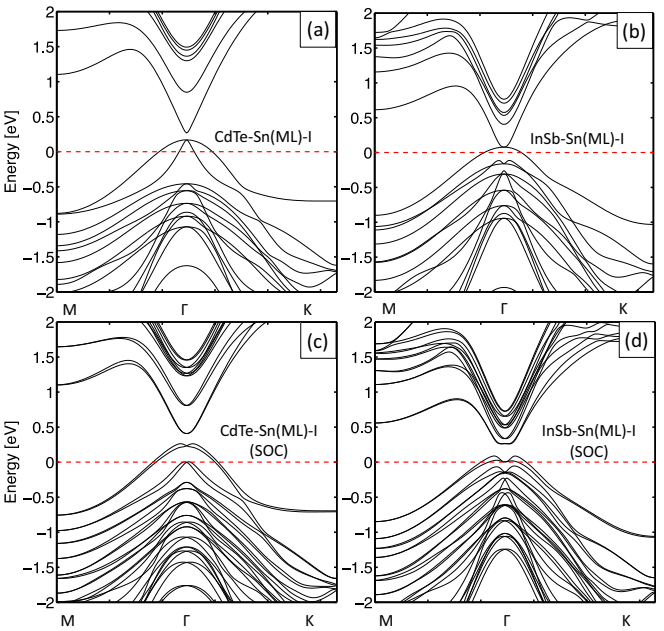

FIG. 5. (Color online) Band structures for (a) CdTe(Cd)-Sn-I, (b) InSb(In)-Sn-I, (c) CdTe(Cd)-Sn-I with SOC, and (d) InSb(In)-Sn-I with SOC. The dashed line (red) indicates the energy of the Fermi level.

Although the full analysis is not shown here for breviety, the InSb(Sb)-Sn-I and CdTe(Te)-Sn-I systems were found to be topological insulators with band gaps of 0.11 and 0.26 eV, respectively.

This trend with respect to the functionalizing agent is similar to the one observed in unsupported halostannanane where I chemisorption also resulted in the largest gap. Although these topological band-gap values are still smaller than those found in the pristine unsupported Sn-MLs (0.34 eV for Sn-ML), these band gaps exceed the thermal energy at room temperature, rendering their use in nanoelectronics possible.

V. CONCLUSIONS

We have studied theoretically the structural and electronic properties of stannene, stannanane, and halostannane films in the presence of a supporting substrate and upon surface functionalization. Three materials were chosen as substrate candidates: Si(111), CdTe(111), and InSb(111). The study of the thermodynamic stability indicated that In-terminated InSb and Cd-terminated CdTe are the most stable substrates, while the use of a Si substrate results in a low-stability system.

The addition of a support led to strain and charge transfer, which induce changes of the electronic properties of the supported Sn-MLs. Stannene supported by a Si substrate led to electronic behavior resembling the high-buckled, metallic, state. Stannene on an InSb support did not exhibit an overall gap and observation of a gap of stannene on a CdTe support is unlikely.

Moreover, charge transfer from the substrate to the tin monolayer led to the intersection of the Fermi level with the conduction or valence band. Upon functionalization with a halogen (X), both InSb-Sn-ML-X and CdTe-Sn-ML-X were shown to be 2D topological insulators, assuming that the

charge transfer by the substrate can be compensated and that the Fermi level can be moved into the gap. InSb-Sn-ML-X and CdTe-Sn-ML-X were further shown to be stable under ultra-high vacuum environments for temperatures below 600 K and 500 K, respectively, and under halogen-rich environments for temperatures below 900 K and 800 K, respectively, rendering their use as 2D topological insulators in nanoelectronics possible.

ACKNOWLEDGMENTS

The authors acknowledge Shela Aboud (Stanford University) and Roberto Longo (UT Dallas) for their advice regarding the *ab initio* simulations and spin-orbit coupling effects. We acknowledge the support of Nanoelectronics Research Initiative's (NRI's) Southwest Academy of Nanoelectronics (SWAN).

[1] M. V. Fischetti, B. Fu, and W. G. Vandenberghe, IEEE Trans. Electron. Device. **60**, 3862 (2013).
[2] Y. Xu, B. Yan, H.-J. Zhang, J. Wang, G. Xu, P. Tang, W. Duan, and S.-C. Zhang, Phys. Rev. Lett. **111**, 136804 (2013).
[3] W. G. Vandenberghe and M. V. Fischetti, J. Appl. Phys. **116**, 173707 (2014).
[4] C.-C. Liu, H. Jiang, and Y. Yao, Phys. Rev. B **84**, 195430 (2011).
[5] Y. Ma, Y. Dai, M. Guo, C. Niu, and B. Huang, J. Phys. Chem. C **116**, 12977 (2012).
[6] J. Seo, P. Roushan, H. Beidenkopf, Y. Hor, R. Cava, and A. Yazdani, Nature **466**, 343 (2010).
[7] Q. Yu, L. A. Jauregui, W. Wu, R. Colby, J. Tian, Z. Su, H. Cao, Z. Liu, D. Pandey, D. Wei *et al.*, Nat. Mater. **10**, 443 (2011).
[8] A. W. Tsen, L. Brown, M. P. Levendorf, F. Ghahari, P. Y. Huang, R. W. Havener, C. S. Ruiz-Vargas, D. A. Muller, P. Kim, and J. Park, Science **336**, 1143 (2012).
[9] M. V. Fischetti and S. Narayanan, J. Appl. Phys. **110**, 083713 (2011).
[10] W. G. Vandenberghe and M. V. Fischetti, in *Electron Devices Meeting (IEDM), 2014 IEEE International* (IEEE, New York, 2014), pp. 33–34.
[11] S.-C. Wu, G. Shan, and B. Yan, Phys. Rev. Lett. **113**, 256401 (2014).
[12] P. Tang, P. Chen, W. Cao, H. Huang, S. Cahangirov, L. Xian, Y. Xu, S.-C. Zhang, W. Duan, and A. Rubio, Phys. Rev. B **90**, 121408 (2014).
[13] P. Rivero, J.-A. Yan, V. M. García-Suárez, J. Ferrer, and S. Barraza-Lopez, Phys. Rev. B **90**, 241408(R) (2014).
[14] K. Ueda, H. Nakayama, M. Sekine, and H. Fujita, Vacuum **42**, 547 (1991).
[15] Y. Ohtsubo, P. Le Fèvre, F. Bertran, and A. Taleb-Ibrahimi, Phys. Rev. Lett. **111**, 216401 (2013).
[16] A. Barfuss, L. Dudy, M. Scholz, H. Roth, P. Höpfner, C. Blumenstein, G. Landolt, J. Dil, N. Plumb, M. Radovic *et al.*, Phys. Rev. Lett. **111**, 157205 (2013).
[17] R. Farrow, D. Robertson, G. Williams, A. Cullis, G. Jones, I. Young, and P. Dennis, J. Cryst. Growth **54**, 507 (1981).
[18] L. L. Wang, X. C. Ma, S. H. Ji, Y. S. Fu, Q. T. Shen, J. F. Jia, K. F. Kelly, and Q. K. Xue, Phys. Rev. B **77**, 205410 (2008).
[19] A. Ohtake, J. Nakamura, T. Eguchi, and T. Osaka, Phys. Rev. B **54**, 10358 (1996).
[20] P. Fantini, S. Gardonio, P. Barbieri, U. del Pennino, C. Mariani, M. G. Betti, E. Magnano, M. Pivetta, and M. Sancrotti, Surf. Sci. **463**, 174 (2000).
[21] G. Kresse and J. Furthmüller, Comp. Mater. Sci. **6**, 15 (1996).
[22] J. P. Perdew, K. Burke, and M. Ernzerhof, Phys. Rev. Lett. **77**, 3865 (1996).
[23] P. E. Blöchl, Phys. Rev. B **50**, 17953 (1994).
[24] H. Monkhorst and J. Pack, Phys. Rev. B **13**, 5188 (1976).
[25] J. Wang, G. Tang, X. Wu, and M. Gu, Thin Solid Films **520**, 3960 (2012).
[26] T. Ohno and K. Shiraishi, Phys. Rev. B **42**, 11194 (1990).
[27] P. Giannozzi, S. Baroni, N. Bonini, M. Calandra, R. Car, C. Cavazzoni, D. Ceresoli, G. L. Chiarotti, M. Cococcioni, I. Dabo, A. Dal Corso, S. de Gironcoli, S. Fabris, G. Fratesi, R. Gebauer, U. Gerstmann, C. Gougoussis, A. Kokalj, M. Lazzeri, L. Martin-Samos, N. Marzari, F. Mauri, R. Mazzarello, S. Paolini, A. Pasquarello, L. Paulatto, C. Sbraccia, S. Scandolo, G. Sclauzero, A. P. Seitsonen, A. Smogunov, P. Umari, and R. M. Wentzcovitch, J. Phys.: Condens. Matter **21**, 395502 (2009).
[28] M. S. Dresselhaus, G. Dresselhaus, and A. Jorio, *Group Theory: Application to the Physics of Condensed Matter* (Springer, Berlin, 2007).
[29] J. C. Garcia, D. B. de Lima, L. V. Assali, and J. F. Justo, J. Phys. Chem. C **115**, 13242 (2011).
[30] L. Fu and C. L. Kane, Phys. Rev. B **76**, 045302 (2007).
[31] J. Wang, X. Wu, and D. Bai, Solid State Commun. **149**, 982 (2009).
[32] Y.-S. Kim, K. Hummer, and G. Kresse, Phys. Rev. B **80**, 035203 (2009).
[33] G. I. Csonka, J. P. Perdew, A. Ruzsinszky, P. H. T. Philipsen, S. Lebègue, J. Paier, O. A. Vydrov, and J. G. Ángyán, Phys. Rev. B **79**, 155107 (2009).
[34] S. B. Zhang and S.-H. Wei, Phys. Rev. Lett. **92**, 086102 (2004).
[35] C. E. Dreyer, A. Janotti, and C. G. Van de Walle, Phys. Rev. B **89**, 081305 (2014).
[36] K. Reuter and M. Scheffler, Phys. Rev. B **65**, 035406 (2001).
[37] J. Evans, P. Thiel, and M. Bartelt, Surf. Sci. Rep. **61**, 1 (2006).
[38] J. Rogal, Ab initio atomistic thermodynamics for surfaces: A primer, Tech. Rep. (DTIC Document, 2006).
[39] A. S. Negreira, S. Aboud, and J. Wilcox, Phys. Rev. B **83**, 045423 (2011).
[40] A. Suarez Negreira and J. Wilcox, J. Phys. Chem. C **117**, 1761 (2013).
[41] C. S. Lo, K. S. Tanwar, A. M. Chaka, and T. P. Trainor, Phys. Rev. B **75**, 075425 (2007).
[42] R.-P. Blum, H. Niehus, C. Hucho, R. Fortrie, M. V. Ganduglia-Pirovano, J. Sauer, S. Shaikhutdinov, and H.-J. Freund, Phys. Rev. Lett. **99**, 226103 (2007).
[43] X.-G. Wang, A. Chaka, and M. Scheffler, Phys. Rev. Lett. **84**, 3650 (2000).
[44] NIST-JANAF, *NIST-JANAF Thermochemical Tables*, 4th ed., edited by J. Chase (American Chemical Society, Washington, DC, 1998).